International Journal of Biological Macromolecules 277 (2024) 134373

Contents lists available at ScienceDirect

International Journal of Biological Macromolecules

journal homepage: www.elsevier.com/locate/ijbiomac

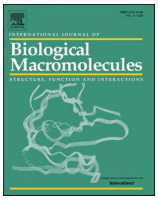

Human ferritin nanocarriers for drug-delivery: A molecular view of the disassembly process

Rosanna Lucignano [a], Gennaro Sanità [b], Emanuela Esposito [b], Irene Russo Krauss [a,c], Anna Maria D'Ursi [d], Michela Buonocore [a,*], Delia Picone [a,*]

[a] Department of Chemical Sciences, University of Naples "Federico II", University of Napoli Federico II Complesso Universitario Monte Sant'Angelo, Via Cintia, 80126 Naples, Italy
[b] Institute of Applied Sciences and Intelligent Systems (ISASI), Naples Cryo Electron Microscopy Laboratory – EYE LAB, National Research Council (CNR), Via Pietro Castellino 111, 80131 Naples, Italy
[c] CSGI (Consorzio per lo Sviluppo dei Sistemi a Grande Interfase), I-50019 Florence, Italy
[d] Department of Pharmacy, University of Salerno, Via Giovanni Paolo II, 132, 84084 Fisciano, Salerno, Italy

ARTICLE INFO

Keywords:
Ferritin nanocages
Nanostructured biomaterials
Protein self-assembly
Human H-chain ferritin
Drug delivery

ABSTRACT

Ferritins are natural proteins which spontaneously self-assemble forming hollow nanocages physiologically deputed to iron storage and homeostasis. Thanks to their high stability and easy production *in vitro*, ferritins represent an intriguing system for nanobiotechnology. Here we investigated the mechanism of disassembly and reassembly of a human recombinant ferritin constituted by the heavy chain (hHFt) exploiting a new procedure which involves the use of minimal amounts of sodium dodecyl sulfate (SDS) and assessed its effectiveness in comparison with two commonly used protocols based on pH shift at highly acidic and alkaline values. The interest in this ferritin as drug nanocarrier is related to the strong affinity of the human H-chain for the transferrin receptor TfR-1, overexpressed in several tumoral cell lines. Using different techniques, like NMR, TEM and DLS, we demonstrated that the small concentrations of SDS can eliminate the nanocage architecture without detaching the monomers from each other, which instead remain strongly associated. Following this procedure, we encapsulated into the nanocage a small ruthenium complex with a remarkable improvement with respect to previous protocols in terms of yield, structural integrity of the recovered protein and encapsulation efficiency. In our opinion, the extensive network of interchain interactions preserved during the SDS-based disassembly procedure represents the key for a complete and correct hHFt reassembly.

1. Introduction

Protein self-assembly is an intriguing process occurring *in vivo*, prompted by physiological or pathological conditions, but also with promising applications in bionanotechnology [1]. Several studies are currently focused on unveiling details about the processes leading to the formation of such ordered multimeric structures to exploit them in applications like engineering, medicine, and materials science [2]. Among spontaneously self-assembling proteins, ferritins appear of particular interest: they are ubiquitous proteins whose physiological function is to protect cells from the damage caused by the Fenton reaction [3] and act as storage systems for iron [4]. All ferritin (Ft) subunits share as a common structural feature a length of about 200 amino acids and a four-helix bundle folding motif. Upon self-assembly, they adopt the quaternary structures typical of this protein class, *i.e.* hollow nanocages, which can be made of 12 subunits in the case of mini-Ft and 24 subunits in the case of maxi-Ft. In particular, maxi-Fts have an outer diameter of roughly 12 nm and an inner diameter of 8 nm, able to store up to 4500 iron atoms [5].

The numerous benefits of using ferritin family proteins in nanotechnology and clinical applications derive from their nature of highly stable compartments to carry and deliver drugs, their biocompatibility, and their sustainable production, which results in high yield, purity, and homogeneity of the protein. Additionally, the surface of the cage can be easily modified or decorated by partial fragment deletion and/or conjugation with a variety of molecules, including small proteins or peptides, obtained by simple alterations of the native sequence while keeping mostly intact the assembly predisposition of the complex [6,7].

* Corresponding authors.
E-mail addresses: michela.buonocore@unina.it (M. Buonocore), delia.picone@unina.it (D. Picone).

https://doi.org/10.1016/j.ijbiomac.2024.134373
Received 7 June 2024; Received in revised form 20 July 2024; Accepted 30 July 2024
Available online 31 July 2024

While the surface decoration may endow the ferritin nanocage with additional functions, such as selective cellular targeting, the removal of part of the polypeptide chains makes in principle easier the passive diffusion of cargo molecules [7], but this advantage is counterbalanced by an uncontrolled drug release.

Another advantage of using Ft in nanotechnology is that the disassembly-reconstitution mechanism is a modular process that can be exploited for several purposes, like drug delivery or pro-drug storage [8]. Indeed, at physiological pH, Ft exists as a stable 24-mer, while in highly acidic or basic solutions it disassembles and, when returned to a neutral solution, the supramolecular complex spontaneously reassembles. This phenomenon can be used to trap molecules in solution within its cavity by dis/assembling ferritin in their presence. By this procedure, described by Ji and co-workers [9], the apo pig pancreas ferritin has been disassembled at basic pH and then reassembled in the presence of the bioactive molecules to trap inside the protein bulk during the reassembly stage. The Ft nanocage disassociation and successive reconstitution were achieved by moving back and forth from pH 7.0 to 13.0 [9,10]. However, this protocol has been applied mostly to horse spleen ferritin [11,12], while no general protocol is experimentally validated for the other ferritins, nor is there a unique shared procedure [13,14]. Additionally, the disassembly with pH shift is somewhat controversial since the protein recovery yield at physiological pH is affected by the precipitation of a significant portion of the sample and heterogeneous reconstitution of the nanocage [15].

Recently, we reported an innovative protocol to disassemble and reassemble homopolymeric Ft nanocages constituted by the heavy chain of the human protein (hHFt) based on the incubation with a denaturing agent, sodium dodecyl sulphate (SDS) at submicellar concentrations [16]. The additional advantage of using this protein as a drug nanocarrier is due to the absence of immunogenicity and the high affinity of H-chains for the transferrin receptor-1 (TfR-1), over-expressed in different cancer cell lines [17], which increases the selectivity for tumor cells.

In this work, we have deeply investigated the disassembly process of hHFt induced by different stressors using a multidisciplinary biophysical approach based on NMR, DLS and native gel electrophoresis, followed by protein reassembly under mild conditions. The comparative analysis allowed us to highlight relevant differences in the disassembling steps and provided a molecular basis to explain the advantages of the SDS-based disassembling procedure, which were further confirmed by the cryo-EM characterization of hHFt nanocages loaded with a Ru-based drug.

2. Results

2.1. Comparative disassembly analysis

The behaviour of hHFt in the presence of already known potential Ft disassembling agents, *i.e.* highly acidic and alkaline pHs and SDS at submicellar concentrations [13,16], was monitored using 1D ^{1}H solution NMR spectroscopy. Indeed, given the big dimensions of the nanocages, only a few low-intensity and broad peaks are detectable in the 1D proton spectrum of the native protein, since the linewidth of the NMR signals increases dramatically as the molecular weight of the sample increases. Hence, we used NMR spectroscopy as a tool to analyze the aggregation state of the protein in a qualitative way, as the appearance of new and/or sharp peaks indicates the presence of smaller-sized protein assemblies or even higher local mobility of side chains. The spectra of hHFt at the concentration of 1.0 mg/mL (2.0 μM) were recorded at 298 K on a Bruker Avance II 500 MHz, while higher resolution spectra were recorded on a Bruker Avance 600 MHz.

To gradually observe the changes in the 1D proton NMR spectra, we report in **Fig. S1** the titration of the hHFt performed by gradual addition of 2 M HCl, 2 M NaOH and 20 % of fully deuterated SDS (SDS_{d25}). The final pHs and the different concentrations of SDS (0.05, 0,075, 0.1 and 0.25 %) are reported on the corresponding spectra. In the acidic titration, the protein profiles are rather similar at pH 7.5, 6.3 and 3.9, suggesting that no significant changes occur in this pH range. Then, at pH 2.0, the intensity of the protein profile abruptly increases (**Fig. S1A**), showing the presence of many peaks, mainly in the aliphatic proton region. Also in the alkaline pH range, substantial changes were observed only at the highest pH (**Fig. S1B**), when the intensity of the spectrum significantly increases. Conversely, the addition of SDS never causes the formation of intense peaks also at the highest detergent concentrations; we only observed, starting from 0.1 % SDS, a modest increase in the intensity of signals in the high-field region (**Fig. S1C**).

To highlight the differences observed in the most significant points of the titrations, we acquired higher resolution 1D ^{1}H NMR spectra with a much higher number of scans to increase the signal to noise (s/n) ratio. A comparative view of the spectra is reported in Fig. 1.

Fig. 1A shows, from the bottom to the top, the stacked 1D ^{1}H NMR spectra of hHFt acquired in native conditions, in the presence of 0.1 % SDS_{d25}, at pH 2.0 and pH 13.0. Magnifications of the low-field and high-field regions are reported in panels **B** and **C**, respectively. In agreement with the previous measurements, the addition of 0.1 % SDS only slightly perturbed the protein profile in the high-field region, corresponding to the aliphatic side chains of apolar amino acids, with the appearance of peaks around 0.96, 1.3, 2.0 and 3.0 ppm (Fig. 1C). Notably, the peaks at 0.84, 1.2, 1.6 and 4.0 ppm belong to residual SDS_{d25} protons (**Fig. S2**). Conversely, in acidic and alkaline conditions, considerably higher intensity and the appearance of large numbers of peaks in the spectrum region corresponding to the aliphatic side chain and backbone protons ($\delta \sim$ 0.5–4.0 ppm) indicates the presence of smaller-size species. Furthermore, at pH 2.0 many signals corresponding to the backbone amide protons (δ = 7.5–9.0 ppm) arise, while at pH 13.0 the peaks belonging to these protons are not present due to the proton/deuterium exchange and signals broadening occurring in very alkaline conditions. However, also in this condition, the profile turns out to be overall much more intense with respect to the native protein.

To confirm the aggregation states of the samples, aliquots of hHFt at pH 2.0, pH 13.0, and in the presence of 0.1 % SDS were analysed by transmission electron microscopy (TEM). The provided data, compared to the images acquired on the untreated protein at the same concentration (Fig. 2A), reported that a nearly quantitative disassembly (> 90 %) occurs in the presence of SDS and at pH 2.0, since only a few nanocages are detectable in panels **B** and **C**. In contrast, at pH 13.0 (Fig. 2D) almost all the nanocages are still present.

2.2. SDS disassembly mechanism

Trying to understand the apparent discrepancies between the NMR data, suggesting that in 0.1 % SDS the hHFt profile is not much different from the one measured under native conditions, and the TEM data, indicating on the other hand that in the presence of the denaturing agent the hHFt nanocage is quantitatively eliminated, we acquired pseudo-2D DOSY spectra to evaluate the dimensions of the aggregates prevalent in 0.1 % SDS and at pH 2.0 and pH 13.0 as a control. These NMR experiments allowed us to measure diffusion values (D, m^2/s, Log_{10} scale) of the solutes and to estimate the molecular size of the samples under scrutiny. For the processing, we monitored the intensity of protein peaks located in 4 representative regions of the spectrum: aliphatic side chain protons (0.4–2.0 ppm), α and β protons (2.5–3.5 ppm), aromatic protons (6.5–7.5 ppm) and amide protons (7.5–8.5 ppm). The region from 3.6 to 6.0 ppm was excluded to avoid picking peaks affected by the water signal decay. In this case, we couldn't use as reference the spectrum of hHFt under native conditions due to the absence of clear DOSY signals, consistent with the very slow diffusion coefficient (**Fig. S3**) of such a high-sized molecule. DOSY spectrum of hHFt disassembled with 0.1 % SDS_{d25} at a protein concentration of 1.0 mg/mL, *i.e.* in the same conditions used for the 1D proton NMR analysis reported in Fig. 1, was equally challenging to obtain. Therefore, we preliminarily acquired

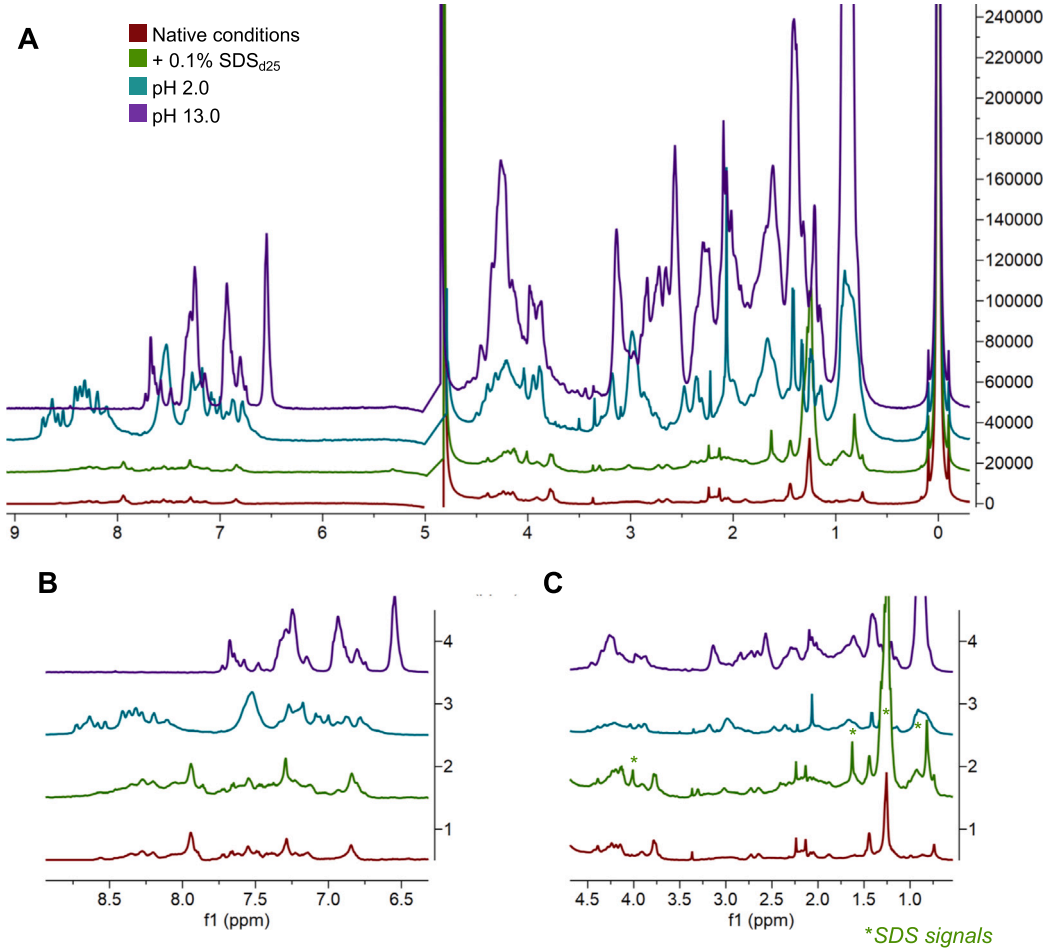

Fig. 1. **A**) 1D ^{1}H NMR of hHFt (1.0 mg/mL) acquired in phosphate buffer 20 mM pH 7.4 (red spectrum) and in the three conditions under scrutiny: after the addition of 0.1 % SDS_{d25} (green spectrum), pH 2.0 (light blue spectrum) and pH 13.0 (purple spectrum). The spectra intensities were normalized on the TSP_{d4} reference peak (1 mM, $\delta = 0.0$ ppm). Zoom on the low-field (**B**) and high-field (**C**) spectral regions, where the intensities are not normalized on the reference peak. The peaks of the residual SDS_{d25} are indicated with an asterisk.

DOSY experiments on hHFt (1.0 mg/mL) in the presence of 0.1 % SDS after 48 h of incubation, hHFt (1.0 mg/mL) with 1.0 % SDS and hHFt (1.5 mg/mL) with 0.1 % SDS. The overlap of the spectra (**Fig. S4**) shows that the protein diffusion is similar in the three conditions, indicating that neither the protein/SDS ratio nor the incubation time over the ranges explored affects the diffusion coefficients of the species detectable in solution. Taking this into account, we recorded DOSY spectra of hHFt in 0.1 % SDS and in the two pH shift conditions using a protein concentration of 1.5 mg/mL (Fig. 3A-B), after checking that also the 1D ^{1}H NMR spectra of hHFt at the 1.5 mg/mL concentration at pH 2.0 and 13.0 are identical to the ones reported in Fig. 1 (data not shown). An increased diffusion value was observed in all the disassembly conditions, indicating that smaller molecular-sized particles are formed. Moreover, the different values observed suggest dissimilar disassembly mechanisms: in fact, the slower diffusions calculated for hHFt in SDS with respect to hHFt at pH 2.0 and pH 13.0 suggest that higher-sized oligomeric species are present in the first case. Conversely, the disassembly based on the pH changes prompts the formation of smaller protein aggregates.

The D values were converted in hydrodynamic radii (r_H) using the known value of dioxane r_H (0.212 nm) [18] as reference in eq. 1, and then converted to hydrodynamic diameter (d_H) by multiplying the obtained value by 2:

$$r_H^{prot} = \frac{D^{ref}}{D^{prot}} r_H^{ref} \quad (1)$$

The result yielded a higher d_H value – 7.58 to 7.94 nm – for hHFt disassembled with 0.1 % SDS compared to the pH shift methods – 4.80 to 5.50 nm –, yet smaller than the diameter of hHFt in native conditions (~12 nm) as experimentally derived from X-ray crystallography [16], and even smaller if considering that d_H values in solutions are larger since they also comprise a hydration shell [18].

Additionally, to have evidence of the sizes of the generated aggregates after treatment with 0.1 % SDS, we performed ultrafiltration of the disassembled sample using a 100 kDa MWCO filter and then loaded the content of the upper cup of the filter and of the flow-through in a polyacrylamide gel under native conditions (Fig. 3C). Visual comparison of untreated hHFt loaded as reference (lanes **1** and **6**), hHFt disassembled in the presence of 0.1 % SDS before ultrafiltration (lane **2**), flow-through (lane **3**) and the content of the upper cup of the filter right after the ultrafiltration (lane **4**) and after dilution with 0.1 % SDS to restore the initial protein concentration (lane **5**) shows that no nanocages were detectable in the samples treated with SDS (lanes **2**, **4** and **5**), where a diffuse band at higher electrophoretic mobility appears. At the same time, we could estimate that the size of the disassembled forms is higher than 100 kDa, since no proteins are found in the flow-through (lane **3**).

We observed the sizes of the nanoparticles in the solution following the disassembly, also by recording dynamic light scattering (DLS) profiles of hHFt before and after treatment with 0.1 % SDS. This technique allowed us to measure the diffusion rate of the protein also in a lower

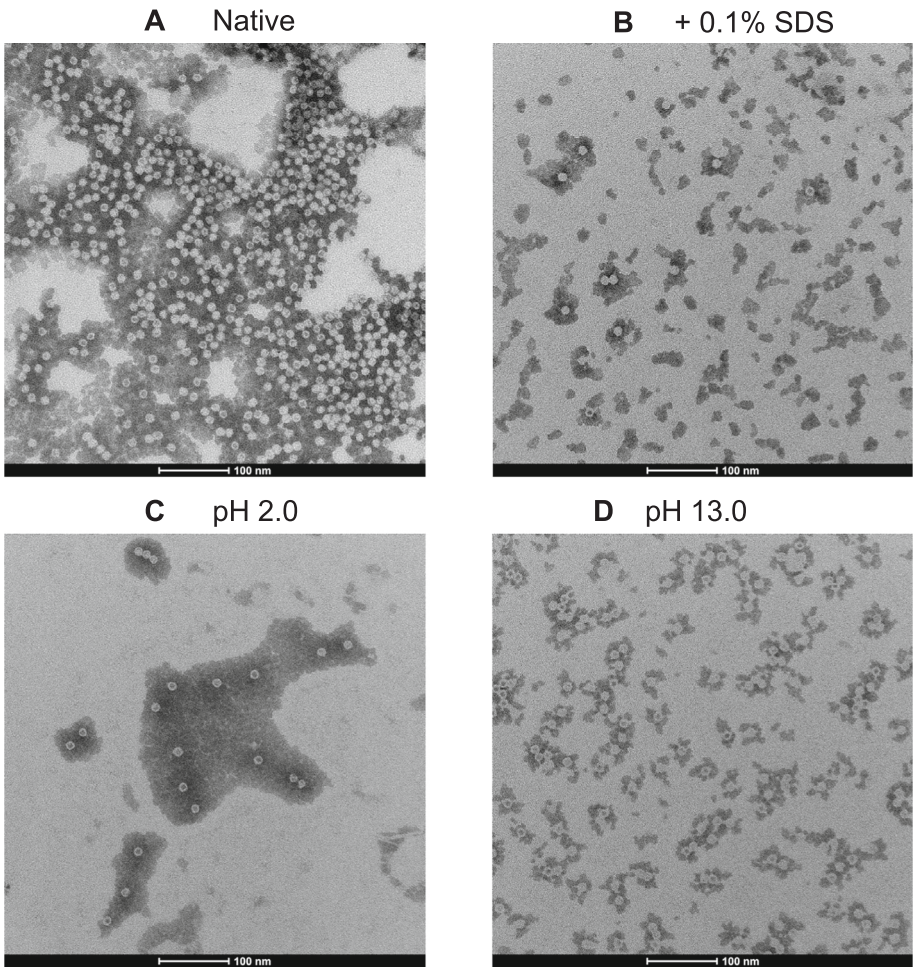

Fig. 2. TEM images (100 nm scale) of the hHFt (0.5 mg/mL) in (**A**) native conditions, (**B**) in the presence of 0.1 % SDS, (**C**) at pH 2.0 and (**D**) 13.0.

concentration, differently from the NMR. Intensity-weighted profiles reported in Fig. 4A show the presence of a main population characterized by $d_H = 21.0 \pm 2.0$ nm and 15.0 ± 0.2 nm for native hHFt and hHFt +0.1 % SDS, respectively, indicating that hHFt treated with the surfactant is smaller than the protein in native conditions. The larger dimensions with respect to the 12 nm reported in the literature can be related to the higher sensitivity of DLS to large objects than to smaller ones, with the intensity proportional to the sixth power of diameter [19], such that the presence of even very small amounts of aggregated Ft is able to shift the distribution towards larger dimension. By analysing volume-weighted profiles, which provide a picture more representative of the actual content of the different species in solution with respect to intensity-weighted profiles, we observe a single population for both native hHFt and hHFt +0.1 % SDS with dimensions of 13 ± 0.5 and 11 ± 0.3 nm respectively (Fig. 4B).

For the sake of comparison, we also analysed hHFt at pH 2.0 and pH 13.0 by means of DLS: in both cases, no clear profile was obtained, likely because of the low scattered light intensity, in turn ascribable to the main presence of smaller objects with respect to native hHFt and hHFt +0.1 % SDS. To get some insights into sample features, we compared the autocorrelation functions of the four hHFt samples, *i.e.* native, SDS-treated, at pH 2.0 and 13.0 (**Fig. S5**). While in the case of native and SDS-treated protein, we observed an autocorrelation function characterized by a single inflection point, index of a monomodal sample with the presence of a single – even if quite broad – population in solution, the autocorrelation functions of hHFt at pH 2.0 and 13.0 are characterized by several inflection points, index of a multimodal sample; in particular, at pH 13.0 the presence of some assembled nanocages can be still inferred by the inflection point at low correlation times, whereas this does not occur for the sample at pH 2.0. The picture emerging from these data is in good agreement with both the 1D spectra and DOSY results.

We also measured the ζ-potential of native hHFt and hHFt +0.1 % SDS in phosphate buffer at pH 7.4, obtaining a value of -20.0 ± 2.0 mV for the native hHFt, a value in good agreement with the anionic features of the protein at pH > pI, and of -50.0 ± 3.0 mV for hHFt with 0.1 % SDS, suggesting a significant interaction of the negatively charged surfactant with the surface of the protein (Fig. 4C).

Altogether, these data suggest that treatment with SDS does not allow the complete disassembly of the protein in its monomeric form or small-sized oligomers, although disrupting the nanocage architecture.

2.3. Reassembly

We examined the behaviour of hHFt after returning to the initial conditions to favour the reassembly of the nanocages. Accordingly, ^{1}H NMR spectra were recorded on the hHFt after the removal of SDS by extensive dialysis and the increase/decrease of pH to 7.4 from pH 2.0 or pH 13.0, respectively (Fig. 5). Remarkably, when brought to pH 7.4 from pH 2.0 and pH 13.0, the protein profiles are not superimposable to the NMR spectrum of the native protein, as some signals remain in the high field region, indicating an incomplete reassembly in both conditions. Differently from the pH shift, the SDS removal does not affect the profile of hHFt, which is entirely superimposable to the 1D spectrum of the protein acquired in native conditions, *i.e.* even the few, small peaks observed upon disassembly (**Fig. S1**) were absent in the reassembled protein.

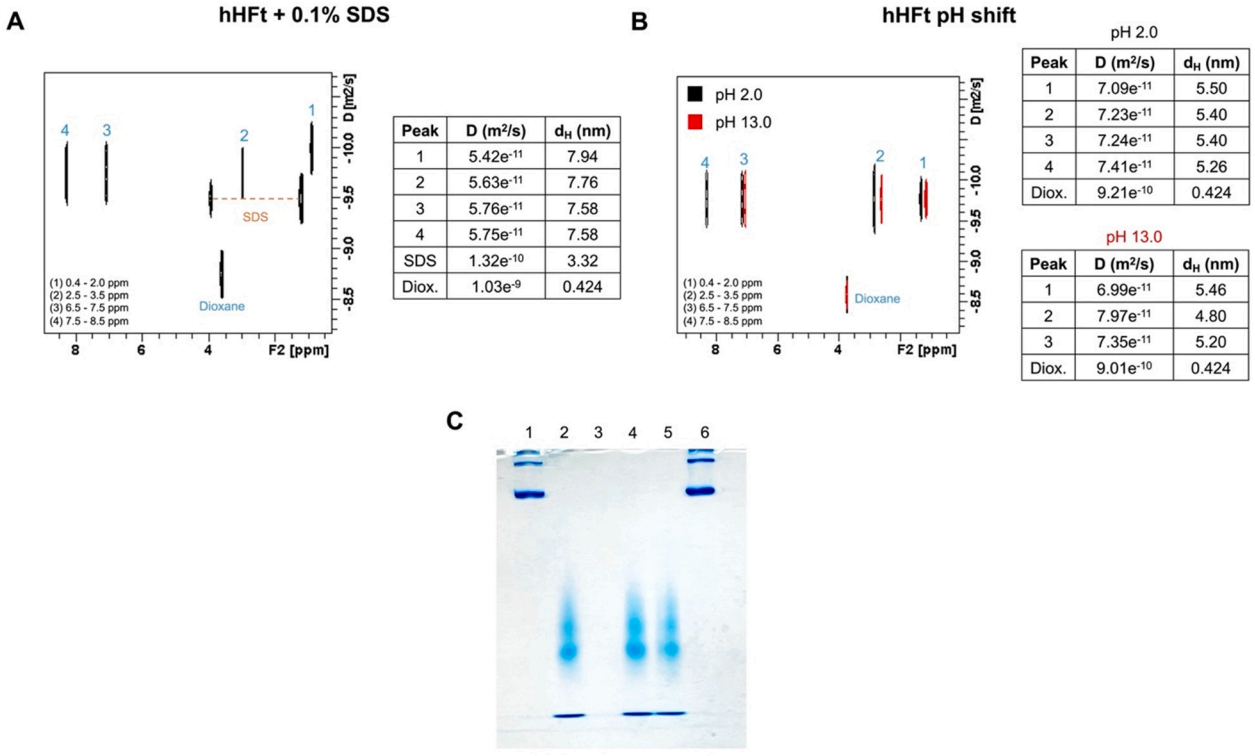

Peak	D (m²/s)	d_H (nm)
1	$5.42e^{-11}$	7.94
2	$5.63e^{-11}$	7.76
3	$5.76e^{-11}$	7.58
4	$5.75e^{-11}$	7.58
SDS	$1.32e^{-10}$	3.32
Diox.	$1.03e^{-9}$	0.424

pH 2.0

Peak	D (m²/s)	d_H (nm)
1	$7.09e^{-11}$	5.50
2	$7.23e^{-11}$	5.40
3	$7.24e^{-11}$	5.40
4	$7.41e^{-11}$	5.26
Diox.	$9.21e^{-10}$	0.424

pH 13.0

Peak	D (m²/s)	d_H (nm)
1	$6.99e^{-11}$	5.46
2	$7.97e^{-11}$	4.80
3	$7.35e^{-11}$	5.20
Diox.	$9.01e^{-10}$	0.424

Fig. 3. Pseudo-2D DOSY spectra correlating the chemical shifts (F2, ppm) with the diffusion values (D, m^2/s, Log_{10} scale), and tables reporting the diffusion values and the deriving hydrodynamic diameters (d_H, nm) of hHFt (1.5 mg/mL) (**A**) in the presence of 0.1 % of SDS, and (**B**) in the pH shift conditions (pH 2.0, black peaks), pH 13.0, red peaks). (**C**) Gel electrophoresis under native conditions of **1** and **6**) untreated hHFt, **2**) hHFt after the treatment with of 0.1 % SDS; **3**) flow through of the disassembled sample after the ultrafiltration with a 100 kDa MWCO filter; **4**) disassembled sample in the upper cup of the filter immediately after the ultrafiltration; **5**) disassembled sample in the upper cup of the filter after dilution with 0.1 % SDS to restore the initial conditions.

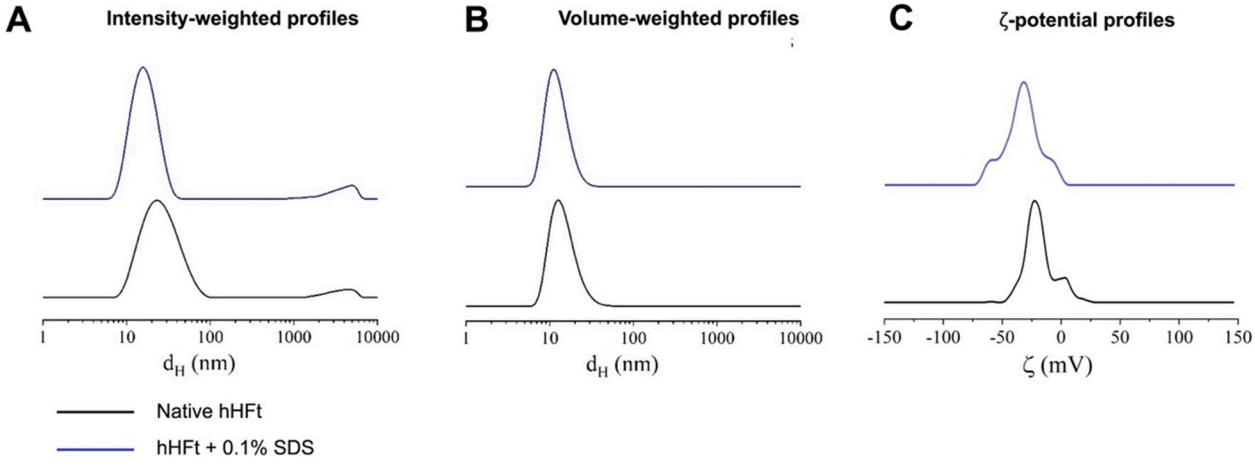

Fig. 4. Dimensions and surface charge of native hHFt (black line) and hHFt in the presence of 0.1 % SDS (blue line). **A**) DLS intensity-weighted profiles, **B**) DLS volume-weighted profiles, **C**) ζ-potential profiles.

To obtain further evidence of the complete reversibility of the SDS-based disassembly and reassembly procedure, an aliquot of hHFt reconstituted after such a procedure was again disassembled by adding 2 M HCl, until pH 2.0. The 1D ^{1}H NMR spectrum of this sample (**Fig. S6B**) was identical to the one of the untreated protein disassembled at pH 2.0 (**Fig. S6C**). Interestingly, the spectrum did not show any of the characteristic signals of SDS, confirming the total removal of the SDS after the disassembly and the reassembly of the nanocages. Differently, the reacquisition after one week of the 1D proton spectra on the hHFt samples after the return to physiological pH following the pH shift (**Fig. S7**) clearly shows that the sharp peaks seen in Fig. 5 do not disappear; therefore, the protein does not return entirely to the initial conditions also after such a considerably long time.

To evaluate the reassembly kinetics, a solution of SDS-treated hHFt diluted ten times with pure buffer to lower the SDS concentration from 0.1 % to 0.01 %, and incubated at different times, was monitored by gel electrophoresis under native conditions in order to follow the aggregation state of the protein and to understand how much time is needed for a complete cage reassembly. Before loading, the samples at different incubation times were were concentrated by ultrafiltration (MWCO 100 kDa) to restore the initial volume. Fig. 6A reports the results obtained after dilution followed by incubation overnight (lane **3**), for 4 h (lane **4**),

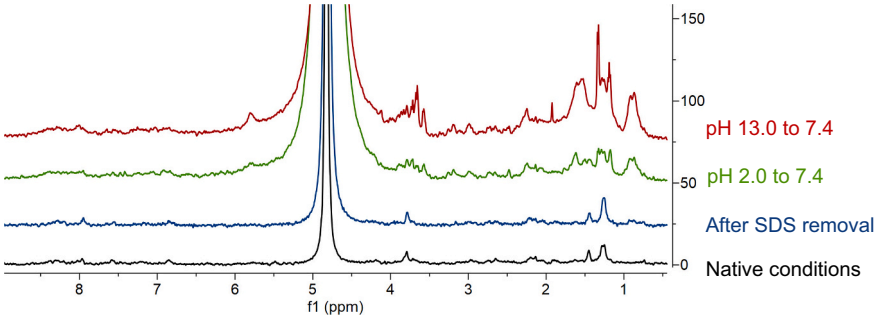

Fig. 5. Spectra of hHFt acquired in native conditions (black spectrum) stacked with the ones acquired after the removal of 0.1 % SDS by dialysis (blue spectrum) and after the return of the protein to physiological pH following the acidic pH shift (green spectrum) and the alkaline pH shift (red spectrum).

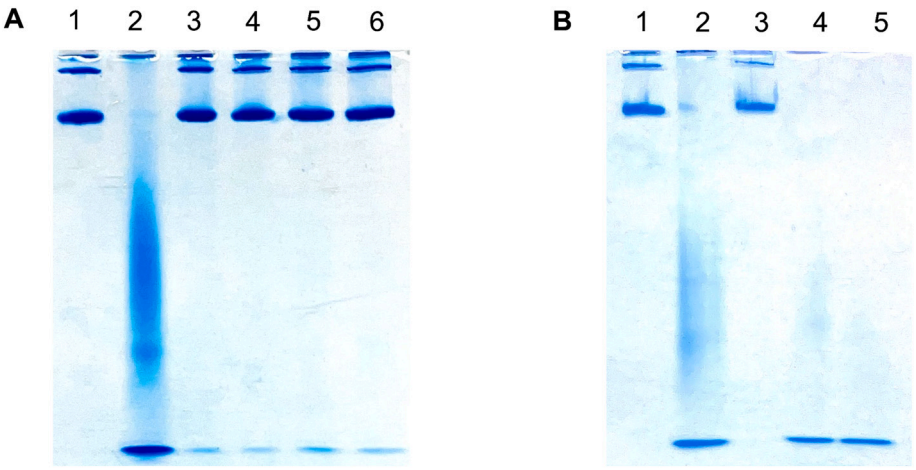

Fig. 6. **A**) Gel electrophoresis under native conditions of untreated hHFt (lane **1**), hHFt +0.1 % SDS (lane **2**), hHFt after dilution to 0.01 % SDS and incubation to allow for reassembly overnight (lane **3**), after 4 h (lane **4**), 2 h (lane **5**) and 1 h (lane **6**); **B**) Gel electrophoresis under native conditions of untreated hHFt (lane **1**), hHFt +0.1 % SDS (lane **2**), hHFt immediately after dilution to 0.01 % SDS (lane **3**), hHFt immediately after dilution to 0.03 % SDS (lane **4**), hHFt immediately after dilution to 0.05 % SDS (lane **5**).

for 2 h (lane **5**) and for 1 h (lane **6**), in comparison with the native protein (lane **1**) and the one treated with 0.1 % SDS (lane **2**). No detectable differences are present between samples in the lanes containing the reassembled protein (lanes **3**–**6**). Indeed, the profiles of hHFt samples reassembled upon different times of incubation following SDS dilution are identical to the one of the untreated protein (lane **1**), indicating that the reassembly is fast and complete after 1 h already, and suggesting that the SDS concentration could instead play a key role. To check the latter hypothesis, we performed a second experiment diluting identical aliquots of disassembled hHFt to the same final volume but reaching different SDS final concentrations: 0.03 % (Fig. 6B, lane **4**) and 0.05 % (Fig. 6B, lane **5**). A sample diluted up to 0.01 % SDS concentration was prepared for comparison (Fig. 6B, lane **3**). This time, hHFt samples were loaded on the gel immediately after dilution to verify the only effect of SDS percentages on the protein reassembly. The obtained results show that a complete reassembly is achieved only when the SDS is diluted up to 0.01 % (lane **3**), whereas at higher SDS concentrations (lanes **4** and **5**), no nanocages are detectable, confirming the previous hypothesis.

We tested the SDS-based protocol efficacy to encapsulate the metal compound Ru1 within the hHFt using a 100:1 metal complex to hHFt cage molar ratio. With respect to the previous protocol [16], here we used a lower metal:protein molar ratio and used a micro-dialysis procedure to slowly decrease the SDS concentration, as described in detail in the experimental section. The obtained nanoparticle consisting of Ru1 within hHFt will be referred to as hHFt-Ru1 in the text. The UV–Vis analysis reported an increase in the absorbance in the 400–500 nm range in the spectrum of free Ru1 (Fig. 7C); this peak is also visible in the spectra of hHFt-Ru1 recorded after the encapsulation protocol, confirming the presence of the metal complex associated with the protein sample (Fig. 7A-B). The protein recovery after the process, calculated using the Bradford assay, was 91 %. To ensure that the drug encapsulation was achieved thanks to the SDS-mediated disassembly and not to the spontaneous diffusion of the metal compound through hHFt pores, we repeated the same procedure without using the SDS. In this case, the UV–Vis spectrum reported in Fig. 7B did not report any increase in absorbance between 400 and 500 nm.

ICP-MS assessed the effective amount of the metal complex within hHFt, yielding a value of 8.3 mol of Ru1 per hHFt cage. ICP-MS measurements confirmed the increased loading capacity, from 4 to about 8 Ru1 molecules encapsulated within the cage (**Table S1**). The encapsulation of the complex Ru1 in the hHFt was observed also with 1D ^{1}H NMR spectroscopy (Fig. 8). For a better comparison, spectra of hHFt-Ru1 before gel filtration (Fig. 8A), after gel filtration (Fig. 8B) and of free Ru1 after gel filtration (Fig. 8C) were acquired. For comparison, we added the spectrum of free Ru1 in Tris-HCl 20 mM pH 7.4 (Fig. 8D). From the results, it is possible to notice that there is a strong reduction in the intensity of Ru1 signals when it is encapsulated in the nanocage, particularly the signals at 7.2, 7.7, 7.9 and 8.4 ppm (**Fig. S8**), while signals at 8.0, 8.3 and 8.4 ppm can be addressed as impurities. The linewidth broadening in signals suggests an interaction with hHFt, which has fast relaxation and slow diffusion and can transfer these parameters to the smaller molecules enclosed in its core. These results provide further evidence of the Ru1 encapsulation within H-chain

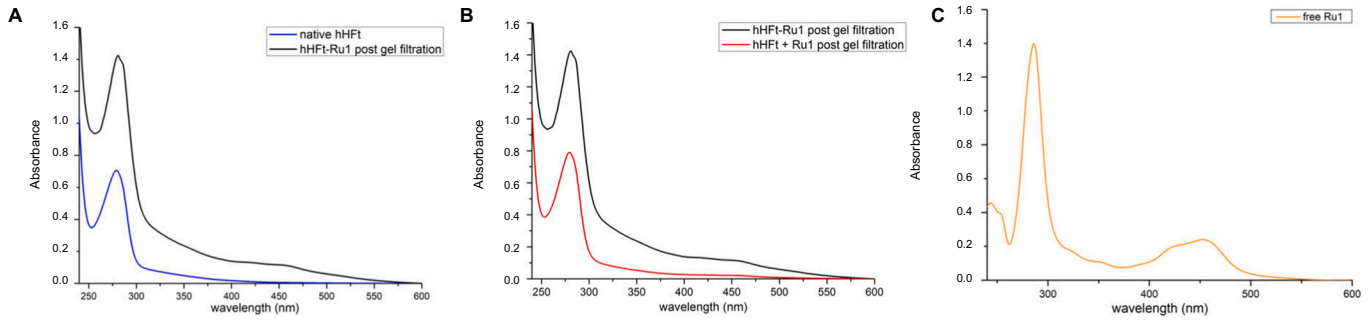

Fig. 7. **A)** UV–Vis spectrum of native hHFt (blue line) overlapped to hHFt-Ru1 after the SDS-based protocol (black line); **B)** UV–Vis spectrum of hHFt-Ru1 after the SDS-based protocol (black line) and of hHFt after the mixing with Ru1 but without the presence of SDS (red line); **C)** UV–Vis spectrum of free Ru1 (10 mM) All the spectra were acquired in 20 mM Tris-HCl pH 7.4.

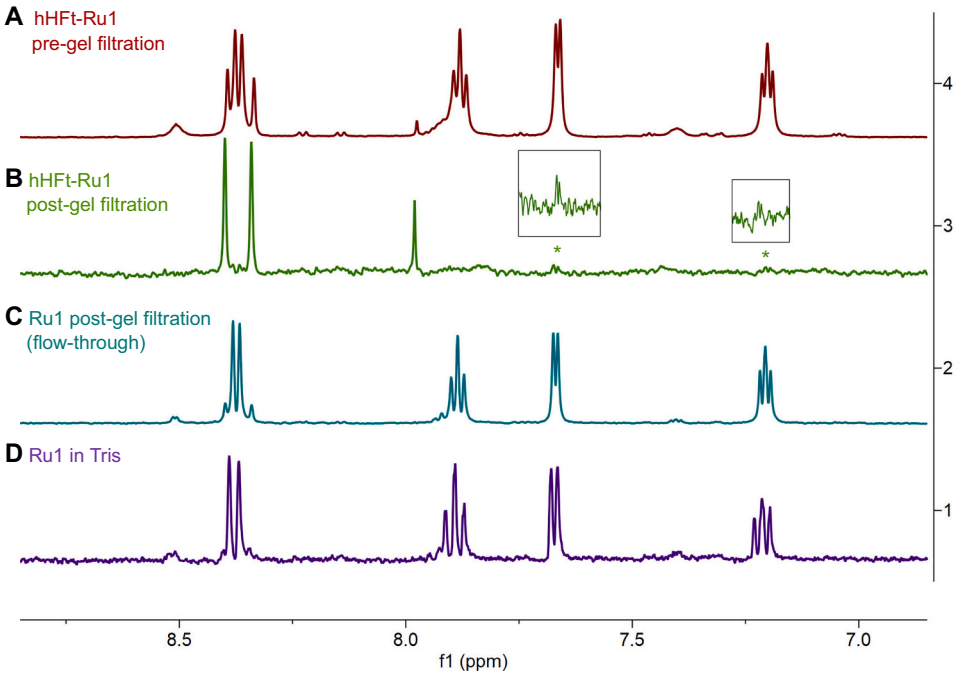

Fig. 8. 1D ^{1}H NMR spectra of (**A**) hHFt-Ru1 after the encapsulation protocol and before gel filtration, (**B**) hHFt-Ru1 after the encapsulation protocol and after gel filtration, (**C**) free Ru1 collected in the gel filtration flow-through solution, and (**D**) free Ru1 dissolved in Tris at pH 7.4 as a comparison.

ferritin nanocages.

Preliminary structure based on Cryo-EM data collected on the hHFt-Ru1 (Fig. 9A) compared to native hHFt (Fig. 9B) indicates, once again, the complete recovery of the original structure upon reassembly. An overlap of both structures is also shown (Fig. 9C).

3. Conclusions

The ability of hHFt to spontaneously self-assemble in a 24-mer utterly stable nanocage makes this protein valuable for a wide variety of nanobiotechnology approaches. It is worth noting its great potential as an effective drug delivery system in many applications, especially in anti-cancer treatments, exploiting its ability to recognize the TfR-1 [17].

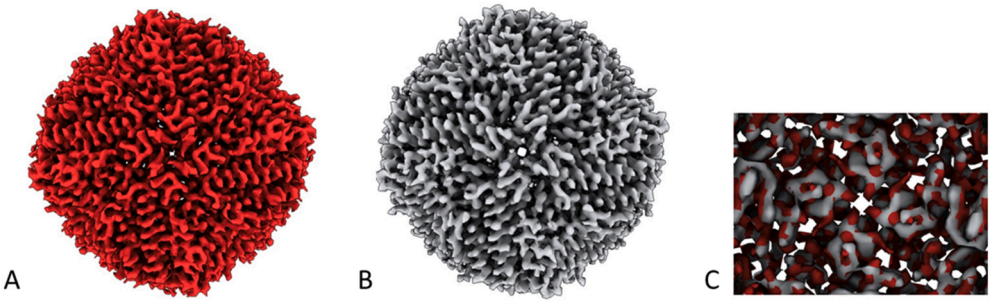

Fig. 9. Cryo-EM structures of **A**) hHFt-Ru1, **B**) native hHFt, **C**) detail of ferritins bulk overlapped.

This possibility critically depends on an efficient and reliable disassembly and reassembly process to achieve an efficient loading with appropriate drugs.

Recently, we have proposed a new disassembly process based on the treatment with SDS under mild denaturing conditions, which allows a quantitative (> 90 %) recovery of a properly folded nanocage [16]. Here, we have deeply investigated the disassembly mechanism induced by SDS compared with other "stressors", *i.e.* incubation at acidic or alkaline pH. NMR experiments indicate that high mobility species are formed when extreme pH values are reached, *i.e.* below 2.5 and above 12.0. (Fig. 1A-C, **Fig. S1A—B**) Under these conditions, only a few nanocages are evident in the TEM images (Fig. 2C) at acidic pH, confirming the quantitative disassembly. However, extensive precipitation is observed, affecting protein recovery. In addition, according to literature data indicating a heterogeneous nanocage reconstitution upon acidic pH dissociation [20], the NMR spectrum of the sample after restoring the pH at physiological values still evidences the presence of some signals typical of highly mobile side chains (Fig. 5), indicating incomplete reassembly.

The incubation at very alkaline pH also induces an extensive change in the 1D proton spectrum (Fig. 1), suggesting the formation of smaller-sized species characterized by high mobility, as also indicated by the diffusion data (Fig. 3B). However, only a few hHFt molecules are affected, *i.e.* the nanocages remain mostly unchanged, as also indicated by TEM images (Fig. 2D), DLS and previous data [16,21]. Last but not least, the extreme pH values required in either case represent a drawback of both protocols, limiting the range of potential cargo molecules to stable ones under such harsh incubation conditions.

Interestingly, all experimental data collected upon incubation in the presence of low SDS concentrations point to an intriguing scenario because, while an extensive disruption of the nanocage architecture is documented by TEM and gel-electrophoresis (Figure2 and 6A-B), no evidence of low molecular weight fragments, *i.e.* monomeric or small-sized oligomeric forms were found. Indeed, only a few signals appear in the 1D proton NMR spectrum, and the diffusion coefficient calculated from the DOSY experiment was definitely lower than the ones obtained at pH 2.0 and 13.0 (Fig. 3A-B), suggesting the presence of high molecular weight assemblies. Accordingly, DLS data indicate that hHFt in the presence of 0.1 % SDS is converted into aggregates smaller than the native protein (Fig. 4), although not as small as the ones formed in the pH shift conditions (**Fig. S5**). Moreover, ultrafiltration of the disassembled hHFt using 0.1 % SDS confirmed that the treatment does not allow the formation of adducts smaller than 100 kDa (Fig. 3C).

Using this SDS-based procedure, we were able to encapsulate into the hHFt shell a small metallo-drug – $[Ru(bpy)_3]^{2+}$ complex (Ru1) – and a 13-residue antimicrobial peptide [16]; however, the cargo size represents another issue in this case, since big-size drugs could hamper the reassembly, while small-size molecules diffusion through the pores during the reassembly could decrease the loading efficiency.

Still, there is room to optimize this aspect. In this work, we have already improved the efficacy of Ru1 encapsulation by hHFt:Ru1 initially decreasing the hHFt:Ru1 molar ratio to 1:100 and reassembling the nanocage by a micro-dialysis against a buffer containing the cargo molecule to prevent its leakage. No precipitation occurred under these conditions, and the protein recovery was quantitative. The amount of Ru1, firstly estimated by UV–Vis (Fig. 7) and then by ICP was, on average, of 8 Ru1 molecules per nanocage, higher than the one we previously reported for the same protein [16] and comparable to the one obtained for the horse-spleen ferritin [22]. Also, the Cryo-EM structure of the reassembled nanocage containing Ru1 was perfectly identical to that of the parent hHFt (Fig. 9), confirming the solidity of our protocol.

A critical aspect of the disassembly procedure based on SDS is represented by the relative amount of protein and surfactant, since a SDS concentration of around 0.1 % can efficiently disassemble hHFt only in a limited protein concentration range, roughly spanning from 1.0 to 3.0 mg/mL [16]. Higher protein concentrations would require higher SDS amounts, which could complicate the removal of the surfactant by simple dilution. Here, we have demonstrated that the SDS concentration represents the crucial parameter to control the aggregation state of the hHFt, whose reassembly can be very fast if the SDS concentration is reduced below 0.01 % by prompt dilution (Fig. 6A-B).

Furthermore, while the conditions we explored are certainly less harsh than the pH shift based procedure, we cannot exclude that the presence of SDS could affect the conformational state and/or the solubility of several cargo molecules, especially proteins, limiting the efficiency of the encapsulation procedure.

In conclusion, we propose that the superior efficiency of the SDS-based protocol presented here relies on the disassembly procedure, which opens the nanocage structures without completely detaching the protein subunits from each other and preventing their precipitation. Unfortunately, we were only able to assess by ultrafiltration that the disassembled form has a size higher than 100 kDa, since DLS could only provide an apparent hydrodynamic diameter pointing to a state of the disassembled nanocage almost undistinguishable from the untreated one. Nonetheless, taken together, the data suggest that the disassembly is rather associated with a change in the shape of the protein, which still preserves an extensive network of interchain interactions. We believe that this extensive network of polypeptide chain interactions represents the molecular basis to prevent protein precipitation and allow the complete and correct reconstitution of the hHFt nanocage when the native conditions are restored.

4. Material and methods

4.1. hHFt production

Human H-chain ferritin was expressed in *E.coli* BL21(DE3). Bacterial cells were transformed with plasmid pET22b+ transferring the gene encoding for the protein. Cells were cultured on LB/Agar containing ampicillin (Amp) 100 mg/L overnight at 37 °C. Afterwards, a single colony was resuspended in LB medium with the same antibiotic overnight at 37 °C, then the starter culture was diluted 1:100 (*v/v*) into LB/Amp and incubated at 37 °C. Protein expression was induced at 0.8 OD_{600}/mL by adding IPTG 0.4 mM and carried for 3 h at 37 °C. Finally, the cells were harvested by centrifugation (4 °C, 8000 rpm, 30′), washed with pure water and stored frozen until protein purification.

4.2. Purification of hHFt

To extract and purify the protein, cells were resuspended in 20 mM Tris-HCl pH 7.4 and sonicated on ice after the addition of anti-protease agents (anti protease Cocktail, Sigma Aldrich, one tablet per 30 mL) with a Microson Ultrasonic Homogenizer XL2000 for 30′ (30″ on 30″ off). Since these proteins are soluble and thermally stable, after sonication, the supernatant was heated at 75 °C for 10 min and centrifuged (4 °C, 12000 rpm, 30′) to remove the precipitated proteins. Then, the solution containing the protein was incubated with 75 μg/mL of DNase and RNase solutions (Sigma Aldrich) for 30′ at 37 °C, centrifuged and loaded on a DEAE anionic exchange column pre-equilibrated with 20 mM Tris-HCl pH 7.4. The column was eluted with a linear gradient of NaCl (0–1.0 M) in the same buffer at a 1.0 mL/min flow rate. The chromatography was monitored by UV absorbance at 280 nm. The fractions containing proteins were pooled and loaded on Sepharose 6B column (2.5 × 24 cm) equilibrated and eluted with 20 mM Tris-HCl pH 7.4. Then, the fractions containing the assembled hHFt nanocages were concentrated by ultrafiltration (MWCO 100 kDa) and stored at 4 °C. Purity of hHFt was assessed by SDS Polyacrylamide Gel Electrophoresis. Protein yield was estimated by UV absorbance at 280 nm and corresponded to about 25 mg per liters of LB medium.

4.3. SDS-based encapsulation of Ru1

0.43 mg of Ru1 powder were added to 2.5 mL of hHFt at 1.0 mg/mL (2 μM) dissociated in 0.1 % SDS, reaching a final concentration of 200 μM. The mixture was stirred for 30 min at RT, until the complex was completely dissolved. Then, the solution was extensively dialyzed against 20 mM Tris-HCl pH 7.4 in the presence of the same concentration of metal compound three times and at RT to decrease the SDS concentration and to achieve the reassembly of the nanocages without reducing the metal concentration. Finally, free Ru1 and residual SDS were removed by gel filtration on a desalting column packed with Sephadex G-25 resin with a loading of 2.5 mL (PD-10, Cytiva®). The protein concentration before and after the treatments was assessed by using the Bradford assay kit (Sigma), using BSA as a standard [23].

4.4. Spectroscopic characterization

UV–Vis absorption spectra were recorded using a 0.1 cm optical path-length quartz cell on a JASCO V-560 UV–Vis spectrophotometer in the range of 240–700 nm, using a protein concentration of 0.25 mg/mL in 10 mM sodium phosphate buffer pH 7.4 and 20 mM Tris-HCl pH 7.4, respectively. Other experimental parameters were bandwidth 2.0 nm, scanning speed 200 nm/min and data pitch 1.0 nm.

4.5. NMR spectroscopy

For the acquisition of the NMR spectra, hHFt samples were prepared in 20 mM sodium phosphate buffer pH 7.4 at the concentrations of 1.5 and 1.0 mg/mL, adding 10 % (*v/v*) of D_2O and 3-(Trimethylsilyl)propionic-2,2,3,3 acid sodium salt-d4 (TSP_{d4}, 1 mM) for the calibration of chemical shifts and intensities to the final solution of 500 μL. 1D, 2D ^1H–^1H total correlation spectroscopy (TOCSY), and pseudo-2D diffusion ordered spectroscopy (DOSY) experiments were recorded at 25 °C on a Bruker Avance II 500 MHz spectrometer equipped with a 5 mm double resonance ^1H—^{13}C inverse BBI probe; high-resolution 1D ^1H spectra were recorded on a Bruker Avance 600 MHz equipped with a 5 mm triple resonance ^1H, ^{13}C and ^{15}N, z-axis pulsed-field gradient probe head. For 1D ^1H experiments, the water signal was suppressed using the WATERGATE gradient pulse (zggpwg) [24], using a D1 of 1 s, 2048–8192 scans for the high-resolution experiments and 64 scans for the monitoring of the reassembly, and a spectral width of 12 ppm. All the spectra were transformed in TopSpin 4.0.9 (Bruker Biospin) and visualized with MNova 9 (MestreLab Research). For pseudo-2D DOSY spectra, we used a sequence of a stimulated echo bipolar pulse field gradient incorporating solvent suppression with WATERGATE (stebpgp1s19) [24]. 2,4-dioxane 1 mM was added to the DOSY samples as a reference. A total of 32 spectra with gradient strengths ranging from 2 % to 98 % of the maximum value were recorded. A diffusion time Δ of 60.0 ms and gradient length δ of 1.0 ms were used in all the experiments. The spectra were analysed using TopSpin Dynamics Center (Bruker, Fällanden, Switzerland). The diffusion values were obtained by fitting the peak intensity decays using the Stejskal-Tanner Eq. [25]. The r_H values were obtained using the Wilkins formula [18] as reported in the results section.

4.6. ICP-AES measurements

The amount of Ru1 encapsulated within hHFt was before estimated by the absorbance at 452 nm, using a molar extinction coefficient of 1.46×10^4 (M^{-1} cm^{-1}) [22] and then measured by multi-element analysis performed by the Inductively Coupled Plasma - Mass Spectrometer (ICP-MS Aurora M90, Bruker, Germany) conducted at the laboratory of Analytical Chemistry for the Environment of the University of Naples Federico II. Nitric acid (HNO_3, 69 % *v/v* Ultratrace@ ppb-trace analysis grade) was provided by Scharlau (Barcelona, Spain). Multi-component solution of 30 elements (10 mg/L each one) was of ultrapure grade for ICP, TraceCERT® and was purchased by Merck (Darmstadt, Germany); ruthenium solution (1.0 mg/L) was of ultrapure grade for ICP, TraceCERT® and was purchased by ROMIL. The analysis was performed in Normal Sensitivity mode. All standards used for analysis in ICP-MS were prepared in HNO_3 solution (2 %, *v/v*). The internal standards were ^{89}Y and ^{115}In for both calibration curve and sample analysis. All the analyses were performed as triplicates.

4.7. TEM analysis

Samples for TEM analysis were prepared by placing a drop of a protein solution (typical concentration 0.5 mg/mL) on a carbon-coated copper TEM grid and allowing the solvent (water) to evaporate. To enhance the contrast, negative staining with 1.5 % phosphotungstic acid (PTA) solution at pH 7.0 was carried out by depositing a drop of PTA solution on the grid containing the sample for 3 min (contact between sample and PTA) and then the excess fluid was drained off with filter paper. The grid was allowed to dry, and images were collected using a FEI TECNAI G2 S-twin apparatus operating at 120 kV (LaB6 source).

4.8. Cryo-EM data acquisition and analysis

Sample for Cryo-EM imaging were prepared using 5 μL of hHFt-Ru1 and of native hHFt, both at a concentration of 0.5 mg/mL in a buffer (20 mM Tris-HCl pH 7.4) solution. The samples were pipetted onto Cryo-EM grids (200 mesh Quantifoil®) that are covered with a holy carbon film (1.2 μm hole size) that was previously made hydrophilic by glow discharge in a low pressure of air. The grids are then blotted with filtered paper for 2 s in 100 % humidity at 4 °C, and rapidly plunge-frozen in liquid ethane cooled by liquid nitrogen; these steps are performed using a dedicated instrument (Vitrobot Mark IV by Thermo Fisher®). A vitreous sample layer fills the holes of the carbon film, then the frozen grids are immediately transferred to a cryo-holder, inserted in the cryo-TEM instrument operated at 200 kV (Glacios by Thermo Fisher® equipped with a Falcon4i Direct Electron Detector camera) and imaged. For structural studies, the micrographs are recorded at a range of defocus settings (0.5 μm, − 1.0 μm and – 1.5 μm) under low electron-dose conditions to minimize beam damage (~ 35 electrons per $Å^2$), then using an energy filter we select only electrons with a specific energy value to form the images (10 eV). About 2000 micrographs for each sample were acquired at a nominal magnification of 79,000 (pixel size of 1.5 Å). As purified proteins usually orient in different ways in vitreous buffer film, their 3D structure can be directly reconstructed by "single particle analysis" of 2D projections obtained [26]. To refine the 3D maps to high resolution of our samples, we used CryoSPARC software and Chimera X. The obtained density maps have a global resolution of 3.79 Å (native hHFt) and 3.37 Å (hHFt-Ru1).

4.9. Dynamic and electrophoretic light scattering (DLS and ELS)

The dimensions of hHFt in native conditions, at pH 2.0, at pH 13.0, in the presence of 0.1 % SDS, and upon SDS removal, as well as the surface charge (ζ-potential) of hHFt in native conditions and in the presence of 0.1 % SDS and upon SDS removal in 20 mM sodium phosphate buffer at pH 7.4 were determined using a Nano ZS zetasizer system (Malvern Instruments) with a laser wavelength of 633 nm (He—Ne). In all the cases, a 1.0 mg/mL protein solution was passed through a 0.2 μm polyvinylidene fluoride (PVDF) membrane before measurement and polystyrene Folded Capillary Zeta cells (Malvern Instruments) were used. Measurement parameters were set as follows: fixed scattering angle of 173°, a medium viscosity of 0.8872 mPa·s and a medium refractive index of 1.330, and material refractive index of 0.200. Each measurement was performed at 25 °C upon a 30 s equilibration time for DLS and 90 s equilibration time for ELS experiments, and the average of five measurements at a stationary level was taken. The zeta potential was calculated by applying the Smoluchowski model [27].

4.10. Disassembly and reassembly on native gel electrophoresis

Disassembly and assembly states of hHFt samples were evaluated by non-denaturing (native) PAGE on a 6 % polyacrylamide gel for the separation, using 25 mM Tris/glycine pH 8.4 as running buffer. For all the gels, hHFt under native conditions and in the presence of 0.1 % SDS were used as reference. Regarding the native PAGE for the disassembly monitoring, hHFt (0.5 mg/mL) was disassembled using 0.1 % SDS and subjected to ultrafiltration using a filter with a 100 kDa MWCO. The flow-through was loaded, while the solution left in the upper cup of the filter was loaded before and after dilution with 0.1 % SDS to restore the initial protein concentration of 0.5 mg/mL. As for the native PAGE for the control of the reassembly kinetics, hHFt (0.5 mg/mL) was disassembled using 0.1 % SDS and then the denaturing agent was diluted to 0.01 %; four aliquots were prepared in which the protein was allowed to reassembly i) overnight, ii) for 4 h, iii) for 2 h and iv) for 1 h. Regarding the native PAGE to monitor the reassembly in the presence of residual SDS, hHFt was disassembled and then allowed to reassembly after diluting SDS concentration from 0.1 % to i) 0.01 %, ii) 0.03 % and iii) 0.05 %. The gels were run for 3.5 h at a constant voltage of 100 V, at 4 °C. Coomassie Brilliant Blue G-250 was used as staining agent [28].

Funding

R. L. was recipient of a fellowship financed by NRRP, PROGETTO PRIN 2022-H37EEZ and M.B. was recipient of a fellowship FRA2022 financed from the Italian Ministry of University and Research (MUR).

CRediT authorship contribution statement

Rosanna Lucignano: Writing – review & editing, Writing – original draft, Visualization, Validation, Methodology, Investigation, Conceptualization. **Gennaro Sanità:** Visualization, Validation, Investigation, Formal analysis. **Emanuela Esposito:** Visualization, Validation, Investigation, Formal analysis. **Irene Russo Krauss:** Writing – review & editing, Validation, Formal analysis. **Anna Maria D'Ursi:** Writing – review & editing, Resources. **Michela Buonocore:** Writing – review & editing, Writing – original draft, Visualization, Validation, Investigation. **Delia Picone:** Writing – review & editing, Writing – original draft, Supervision, Resources, Project administration, Methodology, Conceptualization.

Declaration of competing interest

The authors declare that they have no known competing financial interests or personal relationships that could have appeared to influence the work reported in this paper.

Acknowledgments

We thank Prof. Paola Manini (University of Naples Federico II, Italy) for giving us a sample of the Ru1 complex. We are grateful to MSc Alessandra Marano for assistance with ICP-MS measurements and to MSc Antonella Giarra for her technical support with TEM measurement at the Department of Chemical Sciences, University of Naples Federico II. The financial contribution of University of Naples Federico II for publication fees is acknowledged.

Appendix A. Supplementary data

Supplementary data to this article can be found online at https://doi.org/10.1016/j.ijbiomac.2024.134373.

References

[1] T.A.P.F. Doll, S. Raman, R. Dey, P. Burkhard, Nanoscale assemblies and their biomedical applications, J. R. Soc. Interface 10 (80) (2013).
[2] L.A. Lee, Q. Wang, Adaptations of nanoscale viruses and other protein cages for medical applications, Nanomed-Nanotechnol 2 (3) (2006) 137–149.
[3] S.C. Andrews, The ferritin-like superfamily: evolution of the biological iron storeman from a rubrerythrin-like ancestor, BBA-Gen. Subjects 1800 (8) (2010) 691–705.
[4] N.D. Chasteen, P.M. Harrison, Mineralization in ferritin: an efficient means of iron storage, J. Struct. Biol. 126 (3) (1999) 182–194.
[5] S. Pfaffen, R. Abdulqadir, N.E. Le Brun, M.E.P. Murphy, Mechanism of ferrous Iron binding and oxidation by ferritin from a pennate diatom, J. Biol. Chem. 288 (21) (2013) 14917–14925.
[6] M.Q. Rodrigues, P.M. Alves, A. Roldao, Functionalizing ferritin nanoparticles for vaccine development, Pharmaceutics 13 (10) (2021).
[7] H. Xia, H. Xu, J. Wang, C. Wang, R. Chen, T. Tao, S. Xu, J. Zhang, K. Ma, J. Wang, Heat sensitive E-helix cut ferritin nanocages for facile and high-efficiency loading of doxorubicin, Int. J. Biol. Macromol. 253 (Pt 3) (2023) 126973.
[8] M. Khoshnejad, H. Parhiz, V.V. Shuvaev, I.J. Dmochowski, V.R. Muzykantov, Ferritin-based drug delivery systems: hybrid nanocarriers for vascular immunotargeting, J. Control. Release 282 (2018) 13–24.
[9] X.T. Ji, L. Huang, H.Q. Huang, Construction of nanometer cisplatin core-ferritin (NCC-F) and proteomic analysis of gastric cancer cell apoptosis induced with cisplatin released from the NCC-F, J. Proteome 75 (11) (2012) 3145–3157.
[10] J.M. Dominguez-Vera, Iron(III) complexation of Desferrioxamine B encapsulated in apoferritin, J. Inorg. Biochem. 98 (3) (2004) 469–472.
[11] G. Ferraro, D.M. Monti, A. Amoresano, N. Pontillo, G. Petruk, F. Pane, M. A. Cinellu, A. Merlino, Gold-based drug encapsulation within a ferritin nanocage: X-ray structure and biological evaluation as a potential anticancer agent of the Auoxo3-loaded protein, Chem. Commun. 52 (61) (2016) 9518–9521.
[12] N. Pontillo, F. Pane, L. Messori, A. Amoresano, A. Merlino, Cisplatin encapsulation within a ferritin nanocage: a high-resolution crystallographic study, Chem. Commun. 52 (22) (2016) 4136–4139.
[13] S. Yin, K. Davey, S. Dai, Y.D. Liu, J.X. Bi, A critical review of ferritin as a drug nanocarrier: structure, properties, comparative advantages and challenges, Particuology 64 (2022) 65–84.
[14] K. Krausova, M. Charousova, Z. Kratochvil, P. Takacsova, B. Tesarova, L. Sivak, M. K. Peskova, M. Sukupova, H. Zivotska, P. Makovicky, I. Yamashita, N. Okamoto, D. Hynek, Y. Haddad, V. Pekarik, S. Rex, Z. Heger, Toward understanding the kinetics of disassembly of ferritins of varying origin and subunit composition, Appl. Mater. Today 28 (2022).
[15] M. Kim, Y. Rho, K.S. Jin, B. Ahn, S. Jung, H. Kim, M. Ree, pH-dependent structures of ferritin and Apoferritin in solution: disassembly and reassembly, Biomacromolecules 12 (5) (2011) 1629–1640.
[16] R. Lucignano, I. Stanzione, G. Ferraro, R. Di Girolamo, C. Cane, A. Di Somma, A. Duilio, A. Merlino, D. Picone, A new and efficient procedure to load bioactive molecules within the human heavy-chain ferritin nanocage, Front. Mol. Biosci. 10 (2023).
[17] Y. Shen, X. Li, D.D. Dong, B. Zhang, Y.R. Xue, P. Shang, Transferrin receptor 1 in cancer: a new sight for cancer therapy, Am. J. Cancer Res. 8 (6) (2018) 916–931.
[18] D.K. Wilkins, S.B. Grimshaw, V. Receveur, C.M. Dobson, J.A. Jones, L.J. Smith, Hydrodynamic radii of native and denatured proteins measured by pulse field gradient NMR techniques, Biochemistry 38 (50) (1999) 16424–16431.
[19] A. de Santis, G. Vitiello, M.S. Appavou, E. Scoppola, G. Fragneto, L.C. Barnsley, L. A. Clifton, M.F. Ottaviani, L. Paduano, I. Russo Krauss, G. D'Errico, Not just a fluidifying effect: omega-3 phospholipids induce formation of non-lamellar structures in biomembranes, Soft Matter 16 (46) (2020) 10425–10438.
[20] J.L. Zhang, D.F. Cheng, J.Y. He, J.J. Hong, C. Yuan, M.M. Liang, Cargo loading within ferritin nanocages in preparation for tumor-targeted delivery, Nat. Protoc. 16 (10) (2021) 4878–4896.
[21] R. Lucignano, A. Pratesi, P. Imbimbo, D.M. Monti, D. Picone, L. Messori, G. Ferraro, A. Merlino, Evaluation of Auranofin loading within ferritin Nanocages, Int. J. Mol. Sci. 23 (22) (2022).
[22] X. Li, Y. Zhang, H. Chen, J. Sun, F. Feng, Protein Nanocages for delivery and release of luminescent ruthenium(II) Polypyridyl complexes, ACS Appl. Mater. Interfaces 8 (35) (2016) 22756–22761.
[23] M.M. Bradford, A rapid and sensitive method for the quantitation of microgram quantities of protein utilizing the principle of protein-dye binding, Anal. Biochem. 72 (1976) 248–254.
[24] M. Piotto, V. Saudek, V. Sklenar, Gradient-tailored excitation for single-quantum NMR spectroscopy of aqueous solutions, J. Biomol. NMR 2 (6) (1992) 661–665.
[25] E.O. Stejskal, J.E. Tanner, Spin diffusion measurements: spin echoes in the presence of a time-dependent field gradient, J. Chem. Phys. 42 (1) (1965) 288–292.
[26] J.M. Carazo, C.O. Sorzano, J. Oton, R. Marabini, J. Vargas, Three-dimensional reconstruction methods in single particle analysis from transmission electron microscopy data, Arch. Biochem. Biophys. 581 (2015) 39–48.
[27] G. Ferraro, A. Pica, I. Russo Krauss, F. Pane, A. Amoresano, A. Merlino, Effect of temperature on the interaction of cisplatin with the model protein hen egg white lysozyme, J. Biol. Inorg. Chem. 21 (4) (2016) 433–442.
[28] J.V. Petrak, D. Vyoral, Detection of iron-containing proteins contributing to the cellular labile iron pool by a native electrophoresis metal blotting technique, J. Inorg. Biochem. 86 (4) (2001) 669–675.